Journal Pre-proof

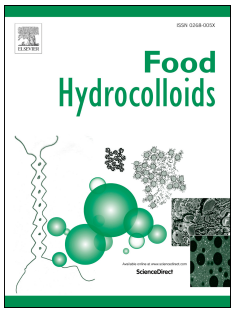

Biobased films of nanocellulose and mango leaf extract for active food packaging: supercritical impregnation versus solvent casting

Cristina Cejudo Bastante, Nuno H.C.S. Silva, Lourdes Casas Cardoso, Casimiro Mantell Serrano, Enrique J. Martínez de la Ossa, Carmen S.R. Freire, Carla Vilela

PII: S0268-005X(21)00125-9

DOI: https://doi.org/10.1016/j.foodhyd.2021.106709

Reference: FOOHYD 106709

To appear in: *Food Hydrocolloids*

Received Date: 29 December 2020

Revised Date: 19 February 2021

Accepted Date: 23 February 2021

Please cite this article as: Bastante, C.C., Silva, N.H.C.S., Cardoso, L.C., Serrano, C.M., Martínez de la Ossa, E.J., Freire, C.S.R., Vilela, C., Biobased films of nanocellulose and mango leaf extract for active food packaging: supercritical impregnation versus solvent casting, *Food Hydrocolloids*, https://doi.org/10.1016/j.foodhyd.2021.106709.

CRediT authorship contribution statement

Cristina Cejudo Bastante: Conceptualization, Investigation, Writing - Original Draft, Writing - Review & Editing

Nuno H. C. S. Silva: Investigation; Writing - review & editing

Lourdes Casas Cardoso: Resources; Writing - review & editing; Funding acquisition

Casimiro Mantell Serrano: Resources; Writing - review & editing; Funding acquisition

Enrique J. Martínez de la Ossa: Resources; Writing - review & editing; Funding acquisition

Carmen S. R. Freire: Resources, Writing - Review & Editing, Supervision, Funding acquisition

Carla Vilela: Conceptualization, Investigation, Writing - Original Draft, Writing - Review & Editing, Supervision

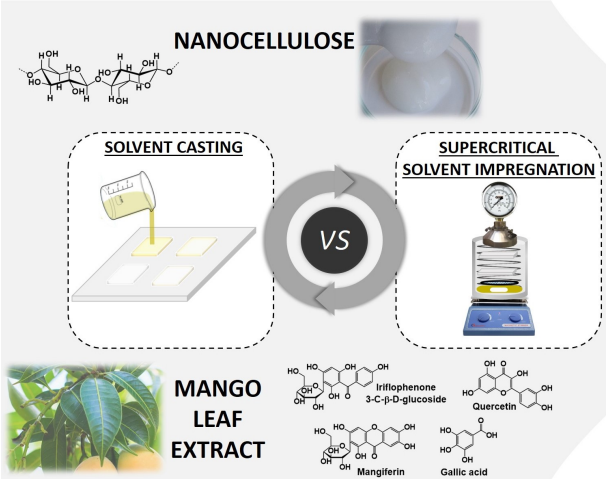

Biobased films of nanocellulose and mango leaf extract for active food packaging: supercritical impregnation versus solvent casting

Cristina Cejudo Bastante [a,*], Nuno H. C. S. Silva [b], Lourdes Casas Cardoso [a], Casimiro Mantell Serrano [a], Enrique J. Martínez de la Ossa [a], Carmen S. R. Freire [b], Carla Vilela [b,*]

[a] Chemical Engineering and Food Technology Department, Wine and Agrifood Research Institute (IVAGRO), University of Cadiz, Cádiz, Spain

[b] CICECO – Aveiro Institute of Materials, Department of Chemistry, University of Aveiro, Aveiro, 3810-193, Portugal

* Corresponding authors: Cristina Cejudo Bastante (cristina.cejudo@uca.es), Carla Vilela (cvilela@ua.pt)

Abstract

Antioxidant and antimicrobial free-standing films composed of nanofibrillated cellulose (NFC) and a polyphenolic-rich extract, *viz*. mango leaf extract (MLE), were produced via supercritical solvent impregnation (SSI) and conventional solvent casting film-processing methodologies. The CO_2-assisted impregnation of NFC with MLE created robust films with thermal stability up to 250 °C, good mechanical performance (Young's modulus > 4.7 GPa), UV-light barrier properties, antioxidant capacity with maximum inhibition percentage of *ca*. 84%, and antimicrobial activity against *Staphylococcus aureus* (growth inhibition ≈ 37%) and *Escherichia coli* (growth inhibition ≈ 91%). The comparison of the NFC/MLE films prepared by SSI with those fabricated via solvent casting shows a clear advantage of the SSI methodology. Particularly, the antioxidant and antimicrobial activities are visibly higher in the films fabricated by the CO_2-assisted impregnation of MLE into NFC. In fact, for the SSI films, the MLE components are mostly adsorbed at the surface and not in the bulk of the biopolymeric matrix, which translates into faster migrations and, hence, higher active properties. All these findings evinced the potential performance of the NFC/MLE films prepared by the eco-friendly SSI as UV-blocking, antioxidant, and antimicrobial bio-based materials for application as sustainable active food packaging.

Keywords: nanocellulose films; mango leaf extract; supercritical solvent impregnation; solvent casting; antioxidant and antimicrobial properties; active food packaging

1. Introduction

The research in the field of active food packaging, *i.e*. packages containing active additives with a key role in food preservation, is mapping a path to boost the safety,

quality and shelf-life of packaged foods by reducing food spoilage, waste and recalls, as well as foodborne illness outbreaks (Carvalho, Freire, & Vilela, 2021; Vilela et al., 2018). Nonetheless, a major part of these active packaging solutions is made of non-biodegradable synthetic polymers and their non-reusable nature gives rise to environmental challenges. Therefore, the use of eco-friendly natural polymers to develop active food packaging systems is one of the promising routes that are being pursued to reduce the environmental impact of disposable packaging materials (Guillard et al., 2018). For example, polysaccharides like chitosan (Vilela et al., 2017; Wang, Qian, & Ding, 2018), pullulan (Farris, Unalan, Introzzi, Fuentes-Alventosa, & Cozzolino, 2014; Kraśniewska, Pobiega, & Gniewosz, 2019; Silva, Vilela, Almeida, Marrucho, & Freire, 2018) and starch (Khan, Niazi, Samin, & Jahan, 2017), are some of the biopolymers already explored for food packaging materials.

Another natural polysaccharide that is starting to garner attention in this domain is cellulose, *viz*. the most abundant biopolymer on earth, and particularly its nanoscale forms, namely nanofibrillated cellulose (NFC), cellulose nanocrystals, and bacterial nanocellulose, as recently reviewed (Azeredo, Rosa, & Mattoso, 2017; Silva, Dourado, Gama, & Poças, 2020). In fact, the low-priced NFC, which is industrially obtained after mechanical disintegration combined with chemical or enzymatic treatments (Heise et al., 2020; Thomas et al., 2018), is a great hydrocolloid contender to design food packaging materials with improved physical, mechanical and barrier properties (Silva et al., 2020).

Equally important is the use of natural compounds or extracts as bioactive additives to convey active properties to the food packaging systems (Carvalho et al., 2021; Vilela et al., 2018), together with the utilization of environmentally friendly film-processing methodologies (Rojas, Torres, Galotto, Guarda, & Julio, 2020; Suhag, Kumar,

Petkoska, & Upadhyay, 2020). The body of literature shows, for example, that the evergreen leaves of *Mangifera indica* L., *viz*. a by-product of the mango fruit industry (Wall-Medrano et al., 2020), are rich in phenolic compounds, including gallic acid, quercetin, iriflophenone 3-C-β-D-glucoside and mangiferin, that present considerable antioxidant and antimicrobial activities (Belizón, Fernández-Ponce, Casas, Mantell, & Ossa-Fernández, 2018; Fernández-Ponce, Casas, Mantell, & Martínez de la Ossa, 2015; Fernández-Ponce, Medina-Ruiz, Casas, Mantell, & Ossa-Fernández, 2018). Hence, the mango leaf extract (MLE) can be explored as a bioactive additive for active food packaging. For instance, Belizón et al. (2018) developed a synthetic multilayer film of poly(ethylene terephthalate) (PET) and polypropylene (PP) loaded with MLE previously obtained by supercritical-assisted extraction. These authors took advantage of an innovative and eco-friendly film-processing methodology, namely the supercritical solvent impregnation (SSI), to impregnate the MLE into a solid hydrophobic and non-biodegradable multilayer PET/PP film (Belizón et al., 2018). The SSI methodology uses supercritical carbon dioxide as the solvent under mild temperature to impregnate the active components (either hydrophilic, hydrophobic or lipophilic compounds) into the polymeric packaging matrix (Mir et al., 2017). This method is gaining increasing attention in the domain of food packaging, mostly for synthetic non-biodegradable (*e.g*., PET, PP) and biodegradable (*e.g*., poly(lactic acid) (PLA) (Milovanovic et al., 2018; Villegas et al., 2017)) polymeric materials, as recently reviewed by Rojas and co-workers (Rojas et al., 2020). Still, little attention has been devoted to the application of the SSI methodology to natural polymers, which is a land of endless opportunities.

In view of our research interest in naturally derived polymeric materials (Vilela, Engström, et al., 2019; Vilela, Moreirinha, et al., 2019), bioactive natural extracts

(Esposito et al., 2020; Vilela et al., 2013), and SSI film-processing methodology (Cejudo Bastante, Casas Cardoso, Fernández Ponce, Mantell Serrano, & Ossa-Fernández, 2018; Cejudo Bastante, Cran, et al., 2019) for food packaging, the purpose of the present study is to develop sustainable films with bioactive functions composed of NFC and MLE via SSI. All films were characterized regarding structure, microstructure, optical properties, thermal stability, mechanical performance, antioxidant capacity and antimicrobial activity. For comparison, the NFC/MLE-based films were also fabricated by the conventional solvent casting film-forming technique, and the advantages and limitations of each film-processing methodology were discussed.

2. Material and methods

2.1. Chemicals, materials, and microorganisms

2,2-Diphenyl-1-picrylhydrazyl (DPPH), glycerol (≥99.5%) and 2,3,5-triphenyl-tetrazolium chloride (TTC, ≥98% for microbiology) were purchased from Sigma-Aldrich (Steinheim, Germany). CO_2 (99.99% purity) used in supercritical experiments was supplied by Abello Linde (Barcelona, Spain). Other solvents were of laboratory grade.

Mangifera Indica L. leaves were supplied by Finca La Mayora (Málaga, Spain). Nanofibrillated cellulose (NFC) suspension (2.91 wt.%), with nanofibrils of 20–50 nm average diameter (HR-SEM-SE SU-70 microscope, Hitachi High-Technologies Corporation, Tokyo, Japan), carboxyl content of 0.14±0.06 mmol g^{-1} (Besbes, Alila, & Boufi, 2011) and zeta potential of *ca*. –13 mV at pH 7 (Zetasizer Nano ZS, Malvern Panalytical, Cambridge, United Kingdom), was supplied by VTT Technical Research

Centre (Espoo, Finland) and obtained from softwood bisulphite fibres by combining mechanical and enzymatic treatments.

Staphylococcus aureus (ATCC 6538) and *Escherichia coli* (CECT101) bacteria were purchased from the American Type Culture Collection (ATCC, Virginia, USA) and the Spanish Type Culture Collection (CECT, Valencia, Spain), respectively.

2.2. Production of the mango leaf extract (MLE)

Magnifera indica L. leaves were dried at room temperature until constant weight and then grounded until *ca*. 5 mm diameter. A cartridge with 160 g of grounded leaves were placed into a 500 mL vessel for supercritical extraction (Thar Technologies SF500, Pittsburgh, PA, USA). The extract was obtained at 200 bar and 80 °C using a 50% ethanol-CO_2 mixture solvent during 2 h at 10 g min^{-1} of total flow, as previously reported (Belizón et al., 2018; Fernández-Ponce et al., 2018). The obtained extract achieved a concentration of 55 g L^{-1}, *viz*. 17.4% extraction yield.

2.3. Production of the NFC/MLE-based films via casting technique

Aqueous suspensions of NFC (2.5%, w/w) were used to fabricate films (5×5 cm^2) containing 50 mg of dried NFC and 10% glycerol (w/w, relative to NFC) by solvent casting (Moreirinha et al., 2020). Films with 10, 20, and 30% of MLE (w/w respecting to the NFC dry content) were produced, as listed in Table 1. The NFC suspensions were sonicated during 30 min and submitted to vacuum during 1 h in order to degas the suspensions. Then, the NFC suspensions were spread into 5×5 cm^2 acrylic moulds and left 24 h at 40 °C in a ventilated oven (Thermo Fisher Scientific, Waltham, MA, USA) to obtain the dried films. Control samples without extract were also developed for comparison purposes.

140

141 *2.4. Production of the NFC/MLE-based films via SSI*

142 The pure NFC films were prepared as previously described for the control samples.
143 Then, samples were impregnated following a procedure similar to that described by
144 Cejudo and co-workers with some modifications (Cejudo Bastante, Cran, et al., 2019).
145 A Thar Technologies SF100 supercritical impregnation equipment (Pittsburgh, PA,
146 USA) was used in the experiments, as depicted in Fig. 1. Two NFC films (5×5 cm^2
147 each) were horizontally disposed into a steal support and introduced in a flat bottom
148 vessel filled with 5 mL of MLE in ethanol (Table 1). An agitator was also inserted to
149 favour the homogenization by a stirring plate fixed at a medium agitation.
150 Pressurization was carried out at 5 g min^{-1} of CO_2 until the pressure/temperature
151 conditions were achieved, and then maintained in the system for 2 h. Once the
152 impregnation time was run, a drying step of the films was required for solvent removal,
153 consisting in applying a CO_2 stream at 5 bar min^{-1} during 20 min. As initial
154 experiments, the depressurization rate (*DR*) was studied in three levels (10, 50 and 100
155 bar min^{-1}), at the most extreme conditions of pressure and temperature (400 bar and 55
156 ºC) without extract addition, in order to verify that the integrity of the matrix remained
157 unaltered. Once determined the most suitable *DR* conditions, *viz*. 10 bar min^{-1}, at which
158 the mechanical properties of the films were preserved without the formation of
159 microbubbles, the impregnation experiments were carried out. The pressure/temperature
160 conditions studied corresponds to an experimental design 2^2, using 100 and 400 bar, and
161 35 and 55 °C.

162

163 *2.5. Characterization methods*

164 *2.5.1. Thickness*

The thickness of the films was measured with a hand-held digital micrometer MDC-25PX (Mitutoyo Corporation, Japan) with an accuracy of 1 μm. All measurements were randomly performed at three different places of the films.

2.5.2. Infrared spectroscopy

The structural analysis of the film's surface was carried out by Fourier transform infrared-attenuated total reflectance (FTIR-ATR) spectroscopy in a Perkin-Elmer FT-IR System Spectrum BX spectrophotometer (Waltham, USA) coupled with a diamond crystal ATR accessory. Each spectrum was the average of 16 scans at a resolution of 4 cm^{-1} and 1 cm^{-1} interval, acquired on a wavelength range from 4000 to 500 cm^{-1}. All spectra were recorded at room temperature and the background spectrum of the clean ATR crystal was collected every 4 samples. Measurements of each sample were repeated twice, and, for data treatment, peaks were normalized at 3600 cm^{-1}.

2.5.3. Scanning electron microscopy (SEM)

Micrographs of the surface and cross-section of the films were obtained by an ultra-high-resolution field-emission HR-FESEM Hitachi SU-70 microscope (Hitachi High-Technologies Corporation, Tokyo, Japan). The samples for surface and cross-section (fractured in liquid nitrogen) examination were placed on a steel plate and coated with a carbon film prior to analysis.

2.5.4. Colour parameters

CIELab parameters were measured using a Konica Minolta CM-2300d portable sphere type spectrophotometer (Konica Minolta Sensing Europe BV, UK) using a white calibration tile surface (Makhloufi et al., 2021). Spectra were collected in three points of

the 5×5 cm^2 films, considering the average of those signals. Duplicate samples were used for each film. The parameters of lightness, L^* (lightness, black (0) to white (100)), as well as colour coordinates, a^* (green= $-a^*$ to red= $+a^*$) and b^* (blue =- b^* to yellow = $+b^*$) were studied and data were obtained using a Spectra Magic™ NX software.

The total colour difference of the films (ΔE) was given by the following equation (Sant'Anna, Gurak, Marczak, & Tessaro, 2013):

$$\Delta E = \sqrt{(\Delta L^*)^2 + (\Delta a^*)^2 + (\Delta b^*)^2}$$

where ΔL^*, Δa^* and Δb^* parameters are the difference between the colour of the pure NFC film and the colour of the NFC/MLE-based films.

2.5.5. Ultraviolet-visible (UV-vis) spectroscopy

For the UV-Vis analysis, the transmittance of the samples was collected with a Shimadzu UV1800 UV–Vis spectrophotometer (Shimadzu Corporation, Kyoto, Japan). Spectra were acquired at room temperature in the wavelength range from 200 to 700 nm in steps of 1 nm.

2.5.6. Thermogravimetric analysis (TGA)

TGA was carried out with a SETSYS Setaram TGA analyser (SETARAM Instrumentation, Lyon, France) equipped with a platinum cell. The samples were heated from 25 to 800 °C at a constant rate of 10 °C min^{-1} under nitrogen atmosphere.

2.5.7. Tensile tests

Tensile properties were measured using an Instron 5966 Series equipment (Instron Corporation, USA) at room temperature, applying a velocity of 10 mm min^{-1} and gauge length of 30 mm, using a static load cell of 500 N. Four specimens of 5×1 cm^2 were

214 measured for each film sample and the average value was considered (ASTM D882).
215 The Instron BlueHill 3 software was used for determining the Young's modulus, tensile
216 strength, and elongation at break data.
217
218 *2.5.8. In vitro antioxidant activity*
219 The *in vitro* antioxidant capacity of the samples was carried out using the DPPH
220 reagent following a methodology described elsewhere (Cejudo Bastante, Casas
221 Cardoso, Mantell Serrano, & Martínez de la Ossa, 2017), and using a Shimadzu
222 UV1800 UV–Vis spectrophotometer (Shimadzu Corporation, Japan). In order to
223 analyse the antioxidant activity of the pure MLE, 100 µL of pure extract at 2000, 4000
224 and 6000 µg mL^{-1} were added to 3.9 mL of a 25 µg mL^{-1} of ethanolic-based DPPH
225 reagent, achieving a final concentration of 50, 100 and 150 µg mL^{-1} of MLE in the final
226 solution. In the case of the film samples, 1 cm^2 of film was introduced into 4 mL of the
227 DPPH solution and was led to diffuse the phenolic compounds during the time of
228 analysis. Analysis were performed in duplicate and the results were expressed as
229 inhibition percentage (I) according to the following equation:

$$I(\%) = \frac{Abs_i - Abs_t}{Abs_i} \times 100$$

230 where Abs_i is absorbance at the initial time and Abs_t is absorbance at time *t* measured at
231 515 nm in each sample.
232
233 *2.5.9. UPLC characterization*
234 Ultra-performance liquid chromatography (UHPLC ACQUITY H Class) coupled to
235 quadrupole-time-of-flight mass spectrometry (QToF-MS) (Xevo G2 QToF, Waters
236 Corp., Milford, MA, USA) was used to identify the phenolic compounds present in the
237 casted and impregnated films. The films were subjected to an extraction using 5 mL of

238 ethanol in an ultrasound bath for 30 min to recover all the incorporated compounds
239 (Fernández-Ponce et al., 2018). To obtain the mass spectra (MS), electrospray operated
240 in negative ionization mode. The mobile phase consisted of a solution of water and
241 0.1% formic acid (solvent A) and acetonitrile and 0.1% formic acid (solvent B).

242 Separation was done using a Acquity UPLC BEH C18 column with a 1.7 µm
243 particle size, working at a constant flow-rate of 0.8 mL min^{-1} during 3 min of total
244 analysis time. Separation started at 98% solvent A during 0.3 min, then decrease until
245 65% at 1.5 min and continuing decreasing until 0% solvent A at 2 min of analysis.
246 Afterwards, the percentage of solvent A was increased again to 98% at 2.5 min and
247 remained at that gradient until end of analysis. The injection volume was 2 µL.

248 For the quantification of MLE compounds, the mass spectra of pure gallic acid,
249 quercetin and mangiferin were obtained according to the method described elsewhere
250 (Fernández-Ponce et al., 2015). Calibration curves were analysed in the range of 0-80
251 µg mL^{-1} (mangiferin: $y = 626.712x + 10609.4$; $r^2 = 0.995$; gallic acid: $y =$
252 $1050.84x + 2019.52$; $r^2 = 0.999$; quercetin: $y = 385.853x + 6710.29$; $r^2 =$
253 0.991). Iriflophenone 3-C-β-D-glucoside was identified by considering the mass
254 fragmentation reported by Fernández-Ponce et al. (2015) and was quantified with the
255 mangiferin calibration curve. Samples were filtered through a 0.2 µm nylon syringe
256 filter and were analysed in duplicate.

257

258 *2.5.10. In vitro antimicrobial activity*

259 The *in vitro* antimicrobial activity against gram-positive (*S. aureus*) and gram-
260 negative (*E. coli*) bacteria was determined according to literature (Cejudo Bastante,
261 Casas Cardoso, Fernández-Ponce, Mantell Serrano, & Martínez de la Ossa, 2019).

The antimicrobial activity of the crude MLE was analysed by plate dilution method by means of a spectrophotometer with a microplate reader (Epoch 2 Biotek, Winooski, VT, USA). Briefly, experiments were carried out in a 96-well plate. Each well was filled with 100 µL of inoculum previously grown in LB broth medium (10^6 CFU mL^{-1}) and 10 µL of the serial diluted MLE and were incubated under the optimal grown conditions (37 °C, 24 h). Then, 10 µL of TTC at 5 mg mL^{-1} was added as bacterial growth indicator. Once added, an incubation period of 30 min was required for the TTC reagent to change its molecular form to 1,3,5-triphenylformazan and, consequently, modify its colour to red, indicating the cell viability (Moussa, Tayel, Al-Hassan, & Farouk, 2013). The absorbance was measured at 500 nm and the analysis were carried out in duplicate. A positive control containing 100 µL of bacteria (10^6 CFU mL^{-1}) and 10 µL of ethanol, and a blank of the ethanolic extract (100 µL of LB medium and 10 µL of MLE) were also measured to determine the percentage of growth inhibition, according to the following equation:

$$Growth\ inhibition\ (\%) = \left(1 - \frac{Abs_i}{Abs_0}\right) \times 100$$

where Abs_i is the absorbance of the samples and Abs_0 is the absorbance of the positive control.

On the other hand, the antimicrobial activity of the NFC/MLE-based films was tested for the NFC/MLE_30 and NFC/MLE_SSI_100-55 films. In each sample, 25 mg of impregnated films were introduced in sterilized tubes with LB broth medium and left for 24 h at 37 °C to promote the diffusion of the MLE compounds from the films into the media. Then, samples were inoculated to achieve a cell concentration of 10^6 CFU mL^{-1} and were incubated for 24 h at 37 °C. A positive control with pure NFC was also carried out to consider any interference of the matrix in the measurements. After the incubation period, the cell concentration in each tube was determined by a McFarland

286 calibration curve carried out with 0.5 to 4 McFarland standards ($C = 14.445T -$
287 0.0962, R^2= 0.9989, where C is the cell concentration and T is turbidity). Then, the
288 percentage of growth inhibition was determined by measuring the turbidity at 625 nm
289 using a UV mini 1240 spectrophotometer (Shimadzu, Japan):

$$Growth\ inhibition\ (\%) = \left(1 - \frac{C_i}{C_0}\right) \times 100$$

290 where C_i is the cell concentration and C_0 is the cell concentration in the medium without
291 film. Analysis was done in duplicate.

292

293 *2.5.11. Statistical analysis*

294 Statistical significance was established at $p < 0.05$ using a one-way variance
295 analysis (ANOVA) and Tukey's test (GraphPad 7.0, GraphPad Software, San Diego,
296 CA, USA).

297

298 **3. Results and discussion**

299 Biobased free-standing films composed of nanofibrillated cellulose (NFC) and
300 mango leaf extract (MLE) were produced via supercritical solvent impregnation (SSI)
301 and conventional solvent casting film-processing methodologies (Fig. 2). The
302 hydrocolloid NFC was selected as the biopolymeric matrix owing to its high surface
303 area and good mechanical performance (Klemm et al., 2018), whereas the MLE
304 polyphenolic-rich extract was chosen for its bioactive properties, namely antioxidant
305 and antimicrobial activities (Belizón et al., 2018; Fernández-Ponce et al., 2015, 2018;
306 Sanchez-Sanchez, Fernández-Ponce, Casas, Mantell, & Martínez de la Ossa, 2017).
307 Furthermore, glycerol was added to improve the handling and flexibility of the
308 NFC/MLE-based films (*i.e.*, 200 μg of glycerol *per* cm^2 of film), given its GRAS

(generally recognized as safe) classification by the FDA (Food and Drug Administration, USA), and thus suitable for food applications.

The SSI methodology was picked for its effectiveness to impregnate solid materials, even with thermolabile solutes, since this high diffusion method operates under low temperatures and originates free-solvent materials (Rojas et al., 2020). The MLE was used in excess, the depressurization rate was selected as 10 bar min^{-1}, and the studied pressure and temperature conditions correspond to an experimental design 2^2, using 100 and 400 bar, and 35 and 55 °C, based on former studies (Belizón et al., 2018; Cejudo Bastante, Cran, et al., 2019). Furthermore, the impregnation yields for those conditions of pressure and temperature are quite high as will be later discussed. For comparison, a pure NFC film and three NFC/MLE films with distinct MLE contents (10, 20 and 30% (w/w) relative to NFC), were prepared following the conventional solvent casting methodology (Fig. 2). As far as we know, this is the first time that NFC films have been enriched with natural extracts, namely mango leaf extract (obtained by supercritical CO_2 extraction), by comparing two different film-processing techniques, for potential application in active food packaging.

The homogenous appearance and straw colour of the NFC/MLE-based films prepared by both methodologies is depicted in Fig. 2. According to Table 1, the thickness values ranged from 17±1 μm for the pure NFC film to 18±1 μm for the films prepared by solvent casting and 19±1 μm for those fabricated by the SSI methodology. All NFC/MLE-based films were characterized regarding structure, microstructure, optical properties, thermal stability, mechanical performance, antioxidant capacity and antimicrobial activity.

3.1. Structure and morphology

The structure of the NFC/MLE-based films was studied by infrared spectroscopy (Fig. 3). According to the FTIR-ATR spectra shown in Fig. 3, the pure NFC film is characterized by the absorption bands of a cellulosic substrate at around 3337 cm^{-1} (vibration of the OH groups), 2898 cm^{-1} (C–H stretching vibrations of CH and CH_2 groups), 1159 cm^{-1} (antisymmetric stretching vibration of the C–O–C glycosidic bonds), and those at 1104, 1052 and 1029 cm^{-1} (stretching vibrations of the C–O bond of carbons 2, 3 and 6) (Foster et al., 2018). On the other hand, the spectrum of the extract (Fig. 3a) presents the characteristic absorption bands of the functional groups of phenolic compounds, the major components of MLE (gallic acid, quercetin, iriflophenone 3-C-β-D-glucoside and mangiferin, Fig. 2), namely at about 3325 cm^{-1} (O–H stretching), 1704 cm^{-1} (C=O stretching), 1608 cm^{-1} (C=C the stretching of the aromatic rings) and 1043 cm^{-1} (C–O stretching) (Samari, Salehipoor, Eftekhar, & Yousefinejad, 2018).

Predictably, the spectra of the NFC/MLE-based films are very similar to that of the pure NFC, independently of the film-processing methodology, because of the low MLE content and the overlap of most of the absorption bands of MLE with those of NFC (Fig. 3a). Furthermore, there is no substantial difference in bands intensity neither on bands shifting, which is an indication that the NFC is merely a physical polymeric matrix that supports the extract. In the case of the casted films, this pattern was previously observed for other biopolymeric-based films containing natural extracts, like for example in the case of the bioactive chitosan-based films containing propolis extract (2.5, 5, 10 and 20% w/w) (Siripatrawan & Vitchayakitti, 2016) and pullulan-based films loaded with polyphenolic-rich extracts (1, 5 and 10% w/w) from chestnut spiny burs and roasted hazelnut skins (Esposito et al., 2020).

The microstructure of the NFC-based films was assessed by SEM as outlined in Fig. 4. The micrographs of the pure NFC film reveal a homogenous surface (Fig. 4a) and a blended mat of entangled nanofibers at the cross-sectional view (Fig. 4b), in accordance with literature (Foster et al., 2018; Moreirinha et al., 2020). When the extract is incorporated into the NFC matrix either by conventional solvent casting or SSI methodology, the surface (Fig. 4a) and cross-section (Fig. 4b) of the films remained almost unaltered with no visible clusters or agglomerates. A similar trend was reported for NFC porous materials obtained by supercritical impregnation of thymol, where the impregnation step had no influence on the microstructure of the ensuing materials (Darpentigny et al., 2020). Furthermore, the cross-sectional micrographs (Fig. 4b) of the NFC/MLE-based films fabricated by both methodologies validate the thickness values listed in Table 1.

3.2. Optical properties

The optical properties of the NFC/MLE-based films were studied regarding their colour parameters and light barrier performance (Fig. 5). According to the CIELab parameters in Fig. 5a, the pure NFC film, with a greenness/redness (a^*) value of 1.10±0.02 and blueness/yellowness (b^*) value of –10.45±0.14, is placed in a different quadrant from all the NFC/MLE-based films, which implies that the MLE, even present in small amounts, contributed to the modification of the colour parameters of the NFC films. A comparable tendency was reported for other polysaccharide-based films (prepared via solvent casting) in which the incorporation of, for instance, phenolic compounds affected the chromatic parameters (a^* and b^*) of the resultant films (Esposito et al., 2020; Siripatrawan & Vitchayakitti, 2016; Vilela et al., 2017).

Additionally, the CIELab parameters of the NFC/MLE-based films prepared by the SSI methodology are different from those produced by the conventional solvent casting technique (Fig. 5a), probably due to their different phenolic composition as will be discussed in section 3.5. Despite the negative contribution to the *a** parameter (green) in the films produced by the two methodologies, the contribution of the *b** parameter is negative (blue) for the films fabricated via SSI and impregnated at 35 °C (*i.e.*, NFC/MLE_SSI_100-35 and NFC/MLE_SSI_400-35), and positive (yellow) for the other two SSI films impregnated at 55 °C (*i.e.*, NFC/MLE_SSI_100-55 and NFC/MLE_SSI_400-55), and for the three films prepared via solvent casting (i.e., NFC/MLE_10, NFC/MLE_20 and NFC/MLE_30). Besides, the positive contribution of parameter *b** (yellow) increased with the increasing content of MLE in the films subjected to casting. In practice, these colour parameters (Fig. 5a) point to films with pale yellowish/greenish colour, which is in harmony with the photographs of the films shown in Fig. 2. Additionally, the lightness (*L**) of the NFC/MLE-based films decreased with the inclusion of the MLE from 92.09±0.07 for the pure NFC to 85.62±1.62 for the NFC/MLE_SSI_100-55. In the case of the films fabricated by conventional solvent casting, the *L** parameter decreased with the increasing content of MLE from 89.46±0.01 for NFC/MLE_10 to 86.52±0.40 for NFC/MLE_30 (Fig. 5a). In regard to the films fabricated by SSI technique, the NFC/MLE_SSI_100-35 is film exhibiting the larger value of lightness (89.07±0.85), while the NFC/MLE_SSI_100-55 presents the lower value (85.62±1.62).

Concerning the total colour difference (ΔE), the NFC/MLE-based films exhibited, as expected, different values depending on the methodology. While the conventional solvent casting originated films with ΔE values of 14.8±0.1 (NFC/MLE_10), 19.1±0.5 (NFC/MLE_20) and 22.2±0.7 (NFC/MLE_30), the SSI technique led to films with ΔE

values of 9.7±1.0 (NFC/MLE_SSI_100-35), 10.8±0.8 (NFC/MLE_SSI_400-35), 11.5±1.6 (NFC/MLE_ SSI_400-55) and 19.5±1.9 (NFC/MLE_SSI_100-55). All these ΔE values indicate a perceptible difference in colour (Mokrzycki & Tatol, 2011), which increased with increasing amount of MLE.

Comprehensibly, the colour parameters will persuade the consumers acceptability towards materials for food packaging (Spence & Velasco, 2018); still, the straw colour of the NFC/MLE-based films fabricated via supercritical solvent impregnation and conventional solvent casting should not be an issue, particularly when compared with the colour of some commercially available packages, like for instance the kraft paper bags known for their brown kraft colour (Gominho, Lopes, Lourenço, Simões, & Pereira, 2014).

The light barrier properties of the NFC/MLE-based films was evaluated by UV-vis spectroscopy in the range of 200-700 nm. According to Fig. 5b, the UV-vis spectrum of the pure NFC film has minimal transmittance values for the full range of wavelengths that increased from *ca*. 4% at 200 nm to *ca*. 30% at 700 nm (Pinto et al., 2020). Quite the opposite, the spectra of MLE at different concentrations (50, 100 and 150 μg mL^{-1}) has low transmittance values in the ultraviolet range but quite high transmittance values in the visible range (400–700 nm). Predictably, the transmittance decreased with the increasing concentration of MLE from 50 to 150 μg mL^{-1} (Fig. 5b).

When the MLE is loaded into the NFC film, the ultraviolet blocking is enhanced particularly in the range of short-wavelength radiation (< 320 nm), independently of the film-processing methodology (Fig. 5c,d). Other studies also reported the increment in the UV-barrier properties when natural extracts are added to biopolymeric matrices. Examples include pullulan-based films containing polyphenolic-rich extracts from chestnut spiny burs and roasted hazelnut skins (Esposito et al., 2020) and chitosan-

based films containing mycosporines extracts of marine organisms (Fernandes et al., 2015).

Another interesting feature is the fact that the three films prepared by conventional solvent casting exhibit lower transmittance values than the pure NFC film for the full range of wavelengths (Fig. 5c), whereas the films prepared by SSI methodology present lower transmittance values in the ultraviolet range but similar or higher transmittance values in the visible range (Fig. 5d). Once more this is probably due to their distinct phenolic composition as will be discussed in section 3.5. Overall, the UV-barrier properties of the NFC/MLE-based films fabricated by both film-processing methodologies are superior to those described, for instance, for the bioactive pullulan-based films containing lysozyme nanofibrils (Silva et al., 2018), chitosan/poly(vinyl alcohol) loaded with lignin nanoparticles (Yang et al., 2016), and chitosan-based films containing ellagic acid (Vilela et al., 2017). In light of the UV-vis data, the low transmittance values of the NFC/MLE-based films vindicate their potential to absorb UV-radiation and, thus, can be labelled as ultraviolet absorbers (secondary or preventive antioxidants) with the ability to avert photo-oxidation of light-sensitive food (Carvalho et al., 2021; Vilela et al., 2018).

3.3. Thermal stability

The thermal stability of the NFC/MLE-based films under inert atmosphere was examined by TGA, and the corresponding data of the pure NFC and the NFC/MLE-based films are compiled in Table 2. The decomposition profile of the pure NFC film follows the typical one-step weight-loss with a maximum rate of decomposition at about 356 °C and a final residue of *ca*. 16% (Pinto et al., 2020). The incorporation of the MLE in the NFC matrix did not have a deleterious effect on the thermal stability of the

ensuing films when compared with the pure NFC film. In fact, the thermal degradation profiles are quite analogous, as demonstrated by the similar initial and maximum rate decomposition temperatures shown in Table 2. Furthermore, the casted and SSI films exhibited a single-step weight-loss profile just like NFC, assigned to the pyrolysis of the cellulosic substrate (Yao et al., 2017), which is the main component of the films.

A comparable stability trend has been reported for other biopolymer-based films containing phytochemicals for application as active food packaging systems (Esposito et al., 2020; Missio et al., 2018; Vilela et al., 2017). The crucial point here is that these NFC/MLE-based films might stand the customary autoclaving sterilization at roughly 120 °C, which is regularly an indispensable condition for materials in contact with food products. Worth mentioning is the fact that the films prepared via SSI might not even require a sterilization step, given that the supercritical CO_2 technology is being applied as an alternative sterilization process in materials used in several domains, including in food applications (Ribeiro et al., 2020).

3.4. Mechanical properties

The mechanical properties of the casted and SSI impregnated NFC/MLE-based films were studied by tensile tests, and the parameters derived from the stress-strain curves, namely the Young's modulus, tensile strength, and elongation at break, are listed in Table 3. As one would expect, the pure NFC film exhibits a Young's modulus of 4.71±0.45 GPa, a tensile strength of 59.7±3.9 MPa and an elongation at break of 3.48±0.95%, in line with data reported in literature (Pinto et al., 2020).

Regarding the NFC/MLE-based films, some differences were observed between the films prepared via conventional solvent casting and SSI methodologies (Table 3). Broadly speaking, all films became stiffer with the incorporation of the polyphenolic-

rich extract in the NFC matrix. On one hand, the Young's modulus of the casted films increased with increasing MLE content, as opposed to the unclear effect or tendency on that parameter in the case of the SSI impregnated films at different pressure and temperature conditions. As specified in Table 3, the Young's modulus values of the casted films are slightly higher than that of the pure NFC film, increasing from 4.98±0.61 GPa for NFC/MLE_10 to 5.64±0.61 GPa for NFC/MLE_30, and, concomitantly, the elongation at break, although already low, slightly decreased from 2.82±0.93% for NFC/MLE_10 to 2.28±0.65% for NFC/MLE_30. An equivalent tendency was reported for bioactive pullulan-based films loaded with polyphenolic-rich extracts from chestnut spiny burs and roasted hazelnut skins (Esposito et al., 2020).

In the case of the films fabricated by SSI, the Young's modulus values are also higher than the pure NFC film, while the tensile strength and elongation at break were marginally affected by the presence of MLE (Table 3). This trend is the opposite of that reported for thermoplastic films composed of poly(lactic acid)/poly(ε-caprolactone) loaded with thymol and/or carvacrol, where the Young's modulus and tensile strength decreased and the elongation at break increased after the supercritical solvent impregnation with thymol and/or carvacrol, which worked as a plasticizer (Lukic, Vulic, & Ivanovic, 2020). Nevertheless, in the present study, the impregnation of NFC with MLE via SSI originated stiffer films with, for example, the NFC/MLE_SSI_400-55 film reaching a Young's modulus of 5.70±0.21 GPa, a tensile strength of 59.4±3.2 MPa and an elongation at break of 3.64±0.91%.

Another interesting feature of the films fabricated by the SSI methodology is that, according to literature, glycerol can be partially solubilized in the supercritical phase and removed after depressurization at lower pressures (Medina-Gonzalez, Tassaing, Camy, & Condoret, 2013), originating a less elastic film. Nevertheless, this is not patent

in the NFC/MLE-based films fabricated herein by the SSI methodology since the values of Young's modulus and elongation at break are all in the same range (Table 3).

Altogether, the mechanical data attest the good mechanical performance of the NFC/MLE-based films, thereby showing that they will probably resist the mechanical pressure to which food packages are susceptible during handling, storage, and transportation, just like the commercially available synthetic polymer materials (Silva et al., 2020).

3.5. Antioxidant activity

The *in vitro* antioxidant activity of the NFC/MLE-based films was determined by the DPPH radical scavenging assay, and the data are compiled in Fig. 6a-c. Not surprisingly, the pure NFC film has no antioxidant activity given the absence of chemical moieties fitted to function as free-radical scavengers (Moreirinha et al., 2020), as opposed to the elevated antioxidant potential of the MLE polyphenolic-rich extract obtained via supercritical-assisted extraction. In fact, the reaction between the DPPH radical and the pure extract (MLE concentrations of the casted films: 50, 100 and 150 μg mL^{-1}) is immediate, reaching inhibition percentages of 55.4±1.7% for the MLE at a concentration of 50 μg mL^{-1} and 86.6±0.5% for the MLE at a concentration of 150 μg mL^{-1}, just after 1 h (Fig. 6a). These results are along the line of the data reported in previous studies (Belizón et al., 2018; Fernández-Ponce et al., 2018; Sanchez-Sanchez et al., 2017).

Regarding the NFC/MLE-based films, all exhibit some level of antioxidant activity but with visible differences between the films prepared via conventional solvent casting (Fig. 6b) and SSI (Fig. 6c) methodologies. In the case of the casted films, the antioxidant activity increased with the augment of the MLE concentration (50, 100 and

150 μg mL^{-1}), which is a common trend among other bioactive polysaccharide-based films (Silva et al., 2018; Vilela et al., 2017). Although the antioxidant activity of the casted films followed the same pattern as the crude extract (*i.e.*, increased with the increasing content of MLE), when the MLE content is lower, namely for NFC/MLE_10 and NFC/MLE_20, a higher diffusion period is required to reach similar inhibition percentages as those found for the pure MLE. Still, the NFC/MLE_30 film was able to achieve comparable results as those found in the pure MLE, with a maximum inhibition percentage of 85.3±1.2% after 24 h. This slow release of MLE from the films with the lower extract content (*i.e.*, NFC/MLE_10 and NFC/MLE_20) is most likely linked with diffusion issues. Actually, the NFC matrix is not water soluble and only disintegrate under vigorous stirring conditions and, hence, it might slow down the MLE diffusion or migration.

In the case of the SSI films, all four films exbibit higher inhibition percentages than the NFC/MLE_10 and NFC/MLE_20 casted films, but comparable inhibition percentages to the NFC/MLE_30 casted film, except for the NFC/MLE_SSI-100-35. Furthermore, a faster initial migration (*i.e.* higher initial slope) is also observed for the SSI films, especially for the films impregnated at 35 °C, which might refer to the lower impact of diffusion issues. This might point to surface deposition/adsorption as the main mechanism for extract incorporation (Rojas et al., 2020). So, if MLE is mostly adsorbed on the surface of the NFC matrix, the migration will be faster (no diffusion issues as for the SSI films) and, therefore, the antioxidant activity will be higher and rapidly reached. Moreover, this higher concentration of MLE at the surface of the SSI films might also contribute to the differences in the colour parameters and UV-vis barrier properties between the films prepared by the two film-processing methodologies.

As reported in literature, the antioxidant activity of the mango leaf extract, obtained by supercritical CO_2-assisted extraction, is ascribed to its phenolic composition, with gallic acid, iriflophenone 3-C-β-D-glucoside, quercetin, and mangiferin as the main components (Belizón et al., 2018; Fernández-Ponce et al., 2015, 2018). Therefore, the composition regarding these four most abundant polyphenols was evaluated for the NFC/MLE_30 casted film, and for the four SSI films, namely NFC/MLE_SSI_100-35, NFC/MLE_SSI_100-55, NFC/MLE_SSI_400-35 and NFC/MLE_SSI_400-55. According to Fig. 6d, the abundance of the polyphenols was higher for all the impregnated films than for the NFC/MLE_30 casted film with just 5.62 mg of phytocompounds *per* g of film, as opposed to a total of 6.87 mg g^{-1} for NFC/MLE_SSI_400-55, 6.97 mg g^{-1} for NFC/MLE_SSI_100-35, 7.72 mg g^{-1} for NFC/MLE_SSI_400-35 and 9.85 mg g^{-1} for NFC/MLE_SSI_100-55. These differences clearly justify the higher antioxidant capacity of all SSI films (Fig. 6c), and, in particular, of the NFC/MLE_SSI_100-55 film that reached a maximum inhibition percentage of 83.9±9.5% after 24 h.

Another interesting aspect is the fact that, when analysing the abundance of the individual phenolic compounds, it is evident that the impregnation seems to exert some kind of selectivity on the content of the impregnated compounds into the NFC matrix. In fact, mangiferin and iriflophenone 3-C-β-D-glucoside, which are the most abundant compounds in MLE (Fernández-Ponce et al., 2015), were also the most abundant ones in the NFC/MLE_30 casted film (Fig. 6d). On the other hand, the minority gallic acid is quite abundant in the SSI film impregnated at 100 bar and 55 ºC conditions (NFC/MLE_SSI-100-55). As regards of mangiferin and quercetin, the casted film (NFC/MLE_30) presented a similar concentration to that of the SSI films, with temperature conditions having a negative and positive impact in the concentration of

581 mangiferin and quercetin, respectively. The most abundant compound is undeniably the
582 iriflophenone 3-C-β-d-glucoside, where the concentration in the impregnated films was
583 significantly higher (from 3.23 mg g^{-1} for NFC/MLE_SSI-100-35 to 4.92 mg g^{-1} for
584 NFC/MLE_SSI_100-55) to that observed for the casted film (1.35 mg g^{-1} for
585 NFC/MLE_30). Notably, the most convenient impregnation conditions were 100 bar
586 and 55 ºC, which offer the higher concentrations of gallic acid, iriflophenone 3-C-β-D-
587 glucoside and quercetin, and, concomitantly, the higher antioxidant activity.

588 On the basis of the antioxidant (Fig. 6c) and UV-barrier (Fig. 5d) properties of the
589 NFC/MLE-based films fabricated by the SSI methodology, it is clear that they have
590 potential as antioxidant food packaging systems to enhance the stability of oxidation-
591 sensitive foods by acting, at the same time, as primary (or chain-breaking) and
592 secondary (or preventive) antioxidant agents with the ability to avoid the occurrence of
593 oxidation reactions (Carvalho et al., 2021; Vilela et al., 2018).

594

595 *3.6. Antimicrobial activity*

596 The analysis of the UV-barrier properties, mechanical performance, and antioxidant
597 activity of the NFC/MLE-based films, motivated the choice of one film from each of the
598 film-processing methodologies, namely NFC/MLE_30 (5.62 mg of phytocompounds
599 *per* g of film) and NFC/MLE_SSI_100-55 (9.85 mg of phytocompounds *per* g of film),
600 to assess their *in vitro* antimicrobial activity against *S. aureus* and *E. coli* bacteria, *viz.*
601 two prevailing pathogenic microorganisms responsible for food poisoning (Hennekinne,
602 De Buyser, & Dragacci, 2012; Kadariya, Smith, & Thapaliya, 2014; S.-C. Yang, Lin,
603 Aljuffali, & Fang, 2017).

604 In a first step, the growth inhibition of the crude MLE and the pure NFC against *S.*
605 *aureus* and *E. coli* was evaluated after 24 h. As shown in Fig. 7a, the MLE inhibited the

growth of both gram-positive and gram-negative bacteria, reaching a growth inhibition of 94.8±3.7% and 99.4±0.9% against *S. aureus* and *E. coli*, respectively, at *ca*. 42 μg mL^{-1} of MLE. This is a major benefit since most polyphenolic-rich extracts exhibit antimicrobial activity against gram-positive bacteria, as opposed to the gram-negative bacteria whose killing mechanism is more difficult due to the higher structural complexity and low permeability of their membranes to phytochemicals (Band & Weiss, 2014; Masi, Réfregiers, Pos, & Pagès, 2017). Still, there are various examples of natural plant extracts with antimicrobial potential towards gram-negative foodborne bacteria (Santos, Martins, Pereira, Silvestre, & Rocha, 2019; S.-C. Yang et al., 2017). The values obtained here for the *E. coli* bacterium are consistent with those reported by Sanchez-Sanchez et al. who also assessed the MLE growth inhibition on *E. coli* (Sanchez-Sanchez et al., 2017). Unsurprisingly, the pure NFC film was not responsible for any bacterial inactivation of *S. aureus* and *E. coli*, as depicted in Fig. 7b, since this nanoscale form of cellulose is not an antimicrobial polymer (Darpentigny et al., 2020; Foster et al., 2018; Thomas et al., 2018).

In the next step, the growth inhibition of the NFC/MLE-based films against *S. aureus* and *E. coli* was also determined, and the differences on their antimicrobial activity towards both bacteria are depicted in Fig. 7b. While the NFC/MLE_30 film presented a growth inhibition of 54.7±16.1% against *S. aureus* and 59.2±13.5% against *E. coli*, the NFC/MLE_SSI_100-55 film prepared via SSI achieved a growth inhibition of 37.0±11.1% against *S. aureus* and 90.9±9.5% against *E. coli* after 24 h. Therefore, the casted film (NFC/MLE_30) has a similar growth inhibition against *S. aureus* and *E. coli* bacteria, contrary to the SSI film (NFC/MLE_SSI_100-55) that has a higher inhibitory effect towards *E. coli*. Just like in the case of the antioxidant activity, there seems to be some kind of hindrance in the migration of the MLE from the films (Fig.

631 7b) when compared with the activity of the crude extract (Fig. 7a). Still, the
632 NFC/MLE_SSI_100-55 film has a good antimicrobial activity when compared with, for
633 example, cellulose acetate films impregnated with thymol via SSI (Zizovic et al., 2018).

634 The antimicrobial potential of the SSI film (NFC/MLE_SSI_100-55) towards the
635 gram-negative bacterium is most definitely credited to the amount and composition of
636 the polyphenolic-rich extract present in the film. As discussed in the previous section,
637 the NFC/MLE_SSI_100-55 film prepared via the SSI methodology is the one showing
638 the higher content of phytochemicals with a total of *ca*. 9.9 mg *per* g of film (Fig. 6d),
639 as well as the larger content of iriflophenone 3-C-β-D-glucoside (*ca*. 4.9 mg *per* g of
640 film), quercetin (*ca*. 2.2 mg *per* g of film) and gallic acid (*ca*. 1.0 mg *per* g of film).
641 According to literature, *S. aureus* is more resistant to quercetin content than *E. coli* (Isa
642 khan et al., 2020), while moringa extracts with a bigger content of gallic acid and
643 quercetin promoted a higher *E. coli* and *S. aureus* inhibition, particularly significant in
644 the growth inhibition of *E. coli* (Sharma, Wichaphon, & Klangpetch, 2020). On the
645 grounds of these results, the NFC/MLE_SSI_100-55 film prepared via the SSI
646 methodology has a great potential as antimicrobial additive for application within the
647 framework of antimicrobial food packaging to inhibit the growth of pathogenic and/or
648 spoilage microorganisms inducing food spoilage (Carvalho et al., 2021; Vilela et al.,
649 2018).

650 The portfolio of biobased NFC/MLE-based films prepared in the present study
651 benefit from a combination of distinct properties covering from UV-light protection and
652 adequate mechanical and thermal properties to antioxidant and antimicrobial activities,
653 which are customizable according to the MLE content and the film-processing
654 methodology. These features or characteristics are apposite in the context of active food
655 packaging since the materials are expected (i) to act as an inert barrier to external

conditions, and (ii) to disclose barrier properties against UV-radiation and antioxidant activity to forestall the risk of photo-oxidation of light-sensitive foods, and antimicrobial activity against pathogenic and/or spoilage microorganisms to reduce or avoid foodborne illness and food spoilage (Carvalho et al., 2021; Vilela et al., 2018).

4. Conclusions

The inclusion of bioactive additives into packaging materials has shown great potential as a valid practice in extending the shelf life of food products. Herein, free-standing robust films composed of nanocellulose and mango leaf extract were manufactured via supercritical solvent impregnation and compared with films prepared by the conventional solvent casting methodology. The CO_2-assisted impregnation of NFC with MLE formed films with thermal stability up to 250 °C, good mechanical performance (Young's modulus > 4.7 GPa), UV-light barrier properties, antioxidant capacity (inhibition percentage ≈ 84%) and antimicrobial activity against *Staphylococcus aureus* (maximum growth inhibition ≈ 55%) and *Escherichia coli* (maximum growth inhibition ≈ 91%). The comparison of the NFC/MLE films prepared by SSI with those produced via conventional solvent casting film-processing methodology shows a clear benefit of the innovative SSI in terms of bioactive properties. In fact, the antioxidant and antimicrobial activities are clearly enhanced in the films fabricated by the CO_2-assisted impregnation of NFC with MLE, whilst the slight improvement of the mechanical performance of the films prepared by SSI. Hence, these outcomes attest the potential performance of the NFC/MLE films fabricated by SSI as UV-blocking, antioxidant, and antimicrobial materials for application as eco-friendly robust active food packaging systems.

Acknowledgments

This work was developed within the scope of the project CICECO-Aveiro Institute of Materials, UIDB/50011/2020 & UIDP/50011/2020, financed by national funds through the Portuguese Foundation for Science and Technology (FCT)/MCTES. FCT is also acknowledged for the research contract under Scientific Employment Stimulus to C. Vilela (CEECIND/00263/2018). The NANOBIOINKS (CENTRO-01-0145-FEDER-031289) project is acknowledged for the research contract of N.H.C.S. Silva. The University of Cadiz is acknowledged for supporting the internship abroad of the researcher C. Cejudo Bastante by the project P18-RT-3272 approved in the FEDER funds 2014-2020.

References

Azeredo, H. M. C., Rosa, M. F., & Mattoso, L. H. C. (2017). Nanocellulose in bio-based food packaging applications. *Industrial Crops and Products*, *97*, 664–671. https://doi.org/10.1016/j.indcrop.2016.03.013

Band, V. I., & Weiss, D. S. (2014). Mechanisms of antimicrobial peptide resistance in gram-negative bacteria. *Antibiotics*, *4*(1), 18–41. https://doi.org/10.3390/antibiotics4010018

Belizón, M., Fernández-Ponce, M. T., Casas, L., Mantell, C., & Ossa-Fernández, E. J. M. de La. (2018). Supercritical impregnation of antioxidant mango polyphenols into a multilayer PET/PP food-grade film. *Journal of CO2 Utilization*, *25*, 56–67. https://doi.org/10.1016/j.jcou.2018.03.005

Besbes, I., Alila, S., & Boufi, S. (2011). Nanofibrillated cellulose from TEMPO-oxidized eucalyptus fibres: Effect of the carboxyl content. *Carbohydrate Polymers*, *84*(3), 975–983. https://doi.org/10.1016/j.carbpol.2010.12.052

706 Carvalho, J. P. F., Freire, C. S. R., & Vilela, C. (2021). Active Packaging. In C.
707 Galanakis (Ed.), *Sustainable food processing and engineering challenges* (1st ed.).
708 Elsevier Science. https://doi.org/10.1016/B978-0-12-822714-5.00009-7
709 Cejudo Bastante, C., Casas Cardoso, L., Fernández-Ponce, M. T., Mantell Serrano, C.,
710 & Martínez de la Ossa, E. J. (2019). Supercritical impregnation of olive leaf extract
711 to obtain bioactive films effective in cherry tomato preservation. *Food Packaging
712 and Shelf Life*, *21*, 100338. https://doi.org/10.1016/j.fpsl.2019.100338
713 Cejudo Bastante, C., Casas Cardoso, L., Fernández Ponce, M. T., Mantell Serrano, C.,
714 & Ossa-Fernández, E. J. M. de la. (2018). Characterization of olive leaf extract
715 polyphenols loaded by supercritical solvent impregnation into PET/PP food
716 packaging films. *The Journal of Supercritical Fluids*, *140*, 196–206.
717 https://doi.org/10.1016/j.supflu.2018.06.008
718 Cejudo Bastante, C., Casas Cardoso, L., Mantell Serrano, C., & Martínez de la Ossa, E.
719 J. (2017). Supercritical impregnation of food packaging films to provide
720 antioxidant properties. *The Journal of Supercritical Fluids*, *128*, 200–207.
721 https://doi.org/10.1016/j.supflu.2017.05.034
722 Cejudo Bastante, C., Cran, M. J., Casas Cardoso, L., Mantell Serrano, C., Martínez de la
723 Ossa, E. J., & Bigger, S. W. (2019). Effect of supercritical CO2 and olive leaf
724 extract on the structural, thermal and mechanical properties of an impregnated food
725 packaging film. *The Journal of Supercritical Fluids*, *145*, 181–191.
726 https://doi.org/10.1016/j.supflu.2018.12.009
727 Darpentigny, C., Marcoux, P. R., Menneteau, M., Michel, B., Ricoul, F., Jean, B., …
728 Nonglaton, G. (2020). Antimicrobial cellulose nanofibril porous materials obtained
729 by supercritical impregnation of thymol. *ACS Applied Bio Materials*, *3*(5), 2965–
730 2975. https://doi.org/10.1021/acsabm.0c00033

731 Esposito, T., Silva, N. H. C. S., Almeida, A., Silvestre, A. J. D., Piccinelli, A., Aquino,
732 R. P., … Freire, C. S. R. (2020). Valorisation of chestnut spiny burs and roasted
733 hazelnut skins extracts as bioactive additives for packaging films. *Industrial Crops*
734 *& Products*, *151*, 112491. https://doi.org/10.1016/j.indcrop.2020.112491
735 Farris, S., Unalan, I. U., Introzzi, L., Fuentes-Alventosa, J. M., & Cozzolino, C. A.
736 (2014). Pullulan-based films and coatings for food packaging: Present applications,
737 emerging opportunities, and future challenges. *Journal of Applied Polymer*
738 *Science*, *131*(13), 40539. https://doi.org/10.1002/app.40539
739 Fernandes, S. C. M., Alonso-Varona, A., Palomares, T., Zubillaga, V., Labidi, J., &
740 Bulone, V. (2015). Exploiting mycosporines as natural molecular sunscreens for
741 the fabrication of UV-absorbing green materials. *ACS Applied Materials &*
742 *Interfaces*, *7*(30), 16558–16564. https://doi.org/10.1021/acsami.5b04064
743 Fernández-Ponce, M. T., Casas, L., Mantell, C., & Martínez de la Ossa, E. (2015). Use
744 of high pressure techniques to produce Mangifera indica L. leaf extracts enriched
745 in potent antioxidant phenolic compounds. *Innovative Food Science and Emerging*
746 *Technologies*, *29*, 94–106. https://doi.org/10.1016/j.ifset.2015.04.006
747 Fernández-Ponce, M. T., Medina-Ruiz, E., Casas, L., Mantell, C., & Ossa-Fernández, E.
748 J. M. (2018). Development of cotton fabric impregnated with antioxidant mango
749 polyphenols by means of supercritical fluids. *The Journal of Supercritical Fluids*,
750 *140*, 310–319. https://doi.org/10.1016/j.supflu.2018.06.022
751 Foster, E. J., Moon, R. J., Agarwal, U. P., Bortner, M. J., Bras, J., Camarero-Espinosa,
752 S., … Youngblood, J. (2018). Current characterization methods for cellulose
753 nanomaterials. *Chemical Society Reviews*, *47*(8), 2609–2679.
754 https://doi.org/10.1039/c6cs00895j
755 Gominho, J., Lopes, C., Lourenço, A., Simões, R., & Pereira, H. (2014). Eucalyptus

globulus stumpwood as a raw material for pulping. *BioResources*, *9*(3), 4038–4049. https://doi.org/10.15376/biores.9.3.4038-4049

Guillard, V., Gaucel, S., Fornaciari, C., Angellier-coussy, H., Buche, P., & Gontard, N. (2018). The Next Generation of Sustainable Food Packaging to Preserve Our Environment in a Circular Economy Context. *Frontiers in Nutrition*, *5*, 121. https://doi.org/10.3389/fnut.2018.00121

Heise, K., Kontturi, E., Allahverdiyeva, Y., Tammelin, T., Linder, M. B., Nonappa, & Ikkala, O. (2020). Nanocellulose : Recent Fundamental Advances and Emerging Biological and Biomimicking Applications. *Advanced Materials*, 2004349. https://doi.org/10.1002/adma.202004349

Hennekinne, J. A., De Buyser, M. L., & Dragacci, S. (2012). Staphylococcus aureus and its food poisoning toxins: characterization and outbreak investigation. *FEMS Microbiology Reviews*, *36*(4), 815–836. https://doi.org/10.1111/j.1574-6976.2011.00311.x

Isa khan, M., Nawaz, M., Bilal Tahir, M., Iqbal, T., Pervaiz, M., Rafique, M., … Alrobei, H. (2020). Synthesis, characterization and antibacterial activity of NiO NPs against pathogen. *Inorganic Chemistry Communications*, *122*, 108300. https://doi.org/10.1016/j.inoche.2020.108300

Kadariya, J., Smith, T. C., & Thapaliya, D. (2014). Staphylococcus aureus and staphylococcal food-borne disease: an ongoing challenge in public health. *BioMed Research International*, *827965*, 1–9. https://doi.org/10.1155/2014/827965

Khan, B., Niazi, M. B. K., Samin, G., & Jahan, Z. (2017). Thermoplastic Starch: A Possible Biodegradable Food Packaging Material—A Review. *Journal of Food Process Engineering*, *40*(3), e12447. https://doi.org/10.1111/jfpe.12447

Klemm, D., Cranston, E. D., Fischer, D., Gama, M., Kedzior, S. A., Kralisch, D., …

781 Rauchfuß, F. (2018). Nanocellulose as a natural source for groundbreaking
782 applications in materials science: Today's state. *Materials Today*, *21*(7), 720–748.
783 https://doi.org/10.1016/j.mattod.2018.02.001
784 Kraśniewska, K., Pobiega, K., & Gniewosz, M. (2019). Pullulan – Biopolymer with
785 potential for use as food packaging. *International Journal of Food Engineering*,
786 *15*(9), 20190030. https://doi.org/10.1515/ijfe-2019-0030
787 Lukic, I., Vulic, J., & Ivanovic, J. (2020). Antioxidant activity of PLA/PCL films
788 loaded with thymol and/or carvacrol using scCO2 for active food packaging. *Food*
789 *Packaging and Shelf Life*, *26*, 100578. https://doi.org/10.1016/j.fpsl.2020.100578
790 Makhloufi, N., Chougui, N., Rezgui, F., Benramdane, E., Freire, C. S. R., Vilela, C., &
791 Silvestre, A. J. D. (2021). Biobased sustainable films from the Algerian Opuntia
792 ficus-indica cladodes powder: effect of plasticizer content. *Journal of Applied*
793 *Polymer Science*, e50450. https://doi.org/10.1002/app.50450
794 Masi, M., Réfregiers, M., Pos, K. M., & Pagès, J. M. (2017). Mechanisms of envelope
795 permeability and antibiotic influx and efflux in Gram-negative bacteria. *Nature*
796 *Microbiology*, *2*(3), 17001. https://doi.org/10.1038/nmicrobiol.2017.1
797 Medina-Gonzalez, Y., Tassaing, T., Camy, S., & Condoret, J. S. (2013). Phase
798 equilibrium of the CO2/glycerol system: Experimental data by in situ FT-IR
799 spectroscopy and thermodynamic modeling. *Journal of Supercritical Fluids*, *73*,
800 97–107. https://doi.org/10.1016/j.supflu.2012.11.012
801 Milovanovic, S., Hollermann, G., Errenst, C., Pajnik, J., Frerich, S., Kroll, S., …
802 Ivanovic, J. (2018). Supercritical CO2 impregnation of PLA/PCL films with
803 natural substances for bacterial growth control in food packaging. *Food Research*
804 *International*, *107*, 486–495. https://doi.org/10.1016/j.foodres.2018.02.065
805 Mir, S. A., Shah, M. A., Dar, B. N., Wani, A. A., Ganai, S. A., & Nishad, J. (2017).

Supercritical Impregnation of Active Components into Polymers for Food Packaging Applications. *Food and Bioprocess Technology*, *10*(9), 1749–1754. https://doi.org/10.1007/s11947-017-1937-9

Missio, A. L., Mattos, B. D., Ferreira, D. de F., Magalhães, W. L. E., Bertuol, D. A., Gatto, D. A., … Tondi, G. (2018). Nanocellulose-tannin films: From trees to sustainable active packaging. *Journal of Cleaner Production*, *184*, 143–151. https://doi.org/10.1016/j.jclepro.2018.02.205

Mokrzycki, W. S., & Tatol, M. (2011). Colour difference ΔE - A survey Mokrzycki. *Machine Graphics and Vision*, *20*(4), 383–411.

Moreirinha, C., Vilela, C., Silva, N. H. C. S., Pinto, R. J. B., Almeida, A., Rocha, M. A. M., … Freire, C. S. R. (2020). Antioxidant and antimicrobial films based on brewers spent grain arabinoxylans, nanocellulose and feruloylated compounds for active packaging. *Food Hydrocolloids*, *108*, 105836. https://doi.org/10.1016/j.foodhyd.2020.105836

Moussa, S. H., Tayel, A. A., Al-Hassan, A. A., & Farouk, A. (2013). Tetrazolium/Formazan Test as an Efficient Method to Determine Fungal Chitosan Antimicrobial Activity. *Journal of Mycology*, 753692. https://doi.org/10.1155/2013/753692

Pinto, R. J. B., Martins, M. A., Lucas, J. M. F., Vilela, C., Sales, A. J. M., Costa, L. C., … Freire, C. S. R. (2020). High-electroconductive nanopapers based on nanocellulose and copper nanowires: a new generation of flexible and sustainable electrical materials. *ACS Applied Materials & Interfaces*, *12*(30), 34208–3416. https://doi.org/10.1021/acsami.0c09257

Ribeiro, N., Soares, G. C., Santos□Rosales, V., Concheiro, A., Alvarez□Lorenzo, C., García□González, C. A., & Oliveira, A. L. (2020). A new era for sterilization

based on supercritical CO2 technology. *Journal of Biomedical Materials Research B*, *108*(2), 399–428. https://doi.org/10.1002/jbm.b.34398

Rojas, A., Torres, A., Galotto, M. J., Guarda, A., & Julio, R. (2020). Supercritical impregnation for food applications: a review of the effect of the operational variables on the active compound loading. *Critical Reviews in Food Science and Nutrition*, *60*(8), 1290–1301. https://doi.org/10.1080/10408398.2019.1567459

Samari, F., Salehipoor, H., Eftekhar, E., & Yousefinejad, S. (2018). Low-temperature biosynthesis of silver nanoparticles using mango leaf extract: catalytic effect, antioxidant properties, anticancer activity and application for colorimetric sensing. *New Journal of Chemistry*, *42*(19), 15905–15916. https://doi.org/10.1039/C8NJ03156H

Sanchez-Sanchez, J., Fernández-Ponce, M. T., Casas, L., Mantell, C., & Martínez de la Ossa, E. J. (2017). Impregnation of mango leaf extract into a polyester textile using supercritical carbon dioxide. *The Journal of Supercritical Fluids*, *128*, 208–217. https://doi.org/10.1016/j.supflu.2017.05.033

Sant'Anna, V., Gurak, P. D., Marczak, L. D. F., & Tessaro, I. C. (2013). Tracking bioactive compounds with colour changes in foods - A review. *Dyes and Pigments*, *98*(3), 601–608. https://doi.org/10.1016/j.dyepig.2013.04.011

Santos, S. A. O., Martins, C., Pereira, C., Silvestre, A. J. D., & Rocha, S. M. (2019). Current challenges and perspectives for the use of aqueous plant extracts in the management of bacterial infections: The case-study of salmonella enterica serovars. *International Journal of Molecular Sciences*, *20*(4), 940. https://doi.org/10.3390/ijms20040940

Sharma, P., Wichaphon, J., & Klangpetch, W. (2020). Antimicrobial and antioxidant activities of defatted Moringa oleifera seed meal extract obtained by ultrasound-

assisted extraction and application as a natural antimicrobial coating for raw chicken sausages. *International Journal of Food Microbiology*, *332*, 108770. https://doi.org/10.1016/j.ijfoodmicro.2020.108770

Silva, F. A. G. S., Dourado, F., Gama, M., & Poças, F. (2020). Nanocellulose bio-based composites for food packaging. *Nanomaterials*, *10*, 2041. https://doi.org/10.3390/nano10102041

Silva, N. H. C. S., Vilela, C., Almeida, A., Marrucho, I. M., & Freire, C. S. R. (2018). Pullulan-based nanocomposite films for functional food packaging: exploiting lysozyme nanofibers as antibacterial and antioxidant reinforcing additives. *Food Hydrocolloids*, *77*, 921–930. https://doi.org/10.1016/j.foodhyd.2017.11.039

Siripatrawan, U., & Vitchayakitti, W. (2016). Improving functional properties of chitosan films as active food packaging by incorporating with propolis. *Food Hydrocolloids*, *61*, 695–702. https://doi.org/10.1016/j.foodhyd.2016.06.001

Spence, C., & Velasco, C. (2018). On the multiple effects of packaging colour on consumer behaviour and product experience in the 'food and beverage' and 'home and personal care' categories. *Food Quality and Preference*, *68*, 226–237. https://doi.org/10.1016/j.foodqual.2018.03.008

Suhag, R., Kumar, N., Petkoska, A. T., & Upadhyay, A. (2020). Film formation and deposition methods of edible coating on food products: A review. *Food Research International*, *136*, 109582. https://doi.org/10.1016/j.foodres.2020.109582

Thomas, B., Raj, M. C., B, A. K., H, R. M., Joy, J., Moores, A., … Sanchez, C. (2018). Nanocellulose, a versatile green platform: from biosources to materials and their applications. *Chemical Reviews*, *118*(24), 11575–11625. https://doi.org/10.1021/acs.chemrev.7b00627

Vilela, C., Engström, J., Valente, B. F. A., Jawerth, M., Carlmark, A., & Freire, C. S. R.

(2019). Exploiting poly(ε-caprolactone) and cellulose nanofibrils modified with latex nanoparticles for the development of biodegradable nanocomposites. *Polymer Composites*, *40*, 1342–1353. https://doi.org/10.1002/pc.24865

Vilela, C., Kurek, M., Hayouka, Z., Röcker, B., Yildirim, S., Antunes, M. D. C., … Freire, C. S. R. (2018). A concise guide to active agents for active food packaging. *Trends in Food Science & Technology*, *80*, 212–222. https://doi.org/10.1016/J.TIFS.2018.08.006

Vilela, C., Moreirinha, C., Domingues, E. M., Figueiredo, F. M. L., Almeida, A., & Freire, C. S. R. (2019). Antimicrobial and conductive nanocellulose-based films for active and intelligent food packaging. *Nanomaterials*, *9*(7), 980. https://doi.org/10.3390/nano9070980

Vilela, C., Pinto, R. J. B., Coelho, J., Domingues, M. R. M., Daina, S., Sadocco, P., … Freire, C. S. R. (2017). Bioactive chitosan/ellagic acid films with UV-light protection for active food packaging. *Food Hydrocolloids*, *73*, 120–128. https://doi.org/10.1016/j.foodhyd.2017.06.037

Vilela, C., Santos, S. A. O., Oliveira, L., Camacho, J. F., Cordeiro, N., Freire, C. S. R., & Silvestre, A. J. D. (2013). The ripe pulp of Mangifera indica L.: A rich source of phytosterols and other lipophilic phytochemicals. *Food Research International*, *54*(2), 1535–1540. https://doi.org/10.1016/j.foodres.2013.09.017

Villegas, C., Torres, A., Rios, M., Rojas, A., Romero, J., Dicastillo, C. L. de, … Guarda, A. (2017). Supercritical impregnation of cinnamaldehyde into polylactic acid as a route to develop antibacterial food packaging materials. *Food Research International*, *99*, 650–659. https://doi.org/10.1016/j.foodres.2017.06.031

Wall-Medrano, A., Olivas-Aguirre, F. J., Ayala-Zavala, J. F., Domínguez-Avila, J. A., Gonzalez-Aguilar, G. A., Herrera-Cazares, L. A., & Gaytan-Martinez, M. (2020).

Health benefits of mango by□products. In R. Campos-Vega, B. D. Oomah, & H. A. Vergara-Castañeda (Eds.), *Food Wastes and By□products: Nutraceutical and Health Potential* (1st ed., pp. 159–191). John Wiley & Sons Ltd. https://doi.org/10.1002/9781119534167.ch6

Wang, H., Qian, J., & Ding, F. (2018). Emerging chitosan-based films for food packaging applications. *Journal of Agricultural and Food Chemistry*, *66*(2), 395–413. https://doi.org/10.1021/acs.jafc.7b04528

Yang, S.-C., Lin, C.-H., Aljuffali, I. A., & Fang, J.-Y. (2017). Current pathogenic Escherichia coli foodborne outbreak cases and therapy development. *Archives of Microbiology*, *199*(6), 811–825. https://doi.org/10.1007/s00203-017-1393-y

Yang, W., Owczarek, J. S., Fortunati, E., Kozanecki, M., Mazzaglia, A., Balestra, G. M., … Puglia, D. (2016). Antioxidant and antibacterial lignin nanoparticles in polyvinyl alcohol/chitosan films for active packaging. *Industrial Crops and Products*, *94*, 800–811. https://doi.org/10.1016/j.indcrop.2016.09.061

Yao, Q., Fan, B., Xiong, Y., Jin, C., Sun, Q., & Sheng, C. (2017). 3D assembly based on 2D structure of cellulose nanofibril/graphene oxide hybrid aerogel for adsorptive removal of antibiotics in water. *Scientific Reports*, *7*(1), 45914. https://doi.org/10.1038/srep45914

Zizovic, I., Senerovic, L., Moric, I., Adamovic, T., Jovanovic, M., Krusic, M. K., … Milovanovic, S. (2018). Utilization of supercritical carbon dioxide in fabrication of cellulose acetate films with anti-biofilm effects against Pseudomonas aeruginosa and Staphylococcus aureus. *Journal of Supercritical Fluids*, *140*, 11–20. https://doi.org/10.1016/j.supflu.2018.05.025

931 **Figure Captions**

932

933 **Fig. 1**. Scheme of the supercritical solvent impregnation (SSI) set-up.

934 **Fig. 2**. Scheme illustrating the fabrication of the biobased NFC/MLE-based films (10
935 wt.% of glycerol) via solvent casting and SSI film-processing methodologies.

936 **Fig. 3**. FTIR-ATR spectra (vibrational mode: ν = stretching) of the pure NFC film, the
937 crude MLE, and the NFC/MLE-based films prepared via solvent casting (a) and SSI (b)
938 film-processing methodologies.

939 **Fig. 4**. SEM micrographs of the (a) surface and (b) cross-section of the NFC-based
940 films.

941 **Fig. 5**. (a) CIELab coordinates of the NFC-based films prepared by solvent casting and
942 SSI film-processing methodologies, (b-d) UV-Vis spectra of (b) NFC and MLE at
943 different concentrations, and NFC-based films prepared via (c) solvent casting and (d)
944 SSI film-processing methodologies.

945 **Fig. 6**. Antioxidant capacity of the (a) pure extracts, and the NFC-based films prepared
946 via (b) solvent casting and (c) SSI film-processing methodologies, and (d) summary of
947 the phenolic composition, in terms of gallic acid, iriflophenone 3-C-β-D-glucoside,
948 quercetin, and mangiferin, of the NFC/MLE-based films obtained by solvent casting
949 and SSI film-processing methodologies (the standard deviation in the duplicates was
950 lower than 5%).

951 **Fig. 7**. Antimicrobial activity against gram-positive (*S. aureus*) and gram-negative (*E.*
952 *coli*) bacteria of the (a) pure MLE and (b) the NFC, NFC/MLE_30 and
953 NFC/MLE_SSI_100-55 films.

954

955

956 **Figures**

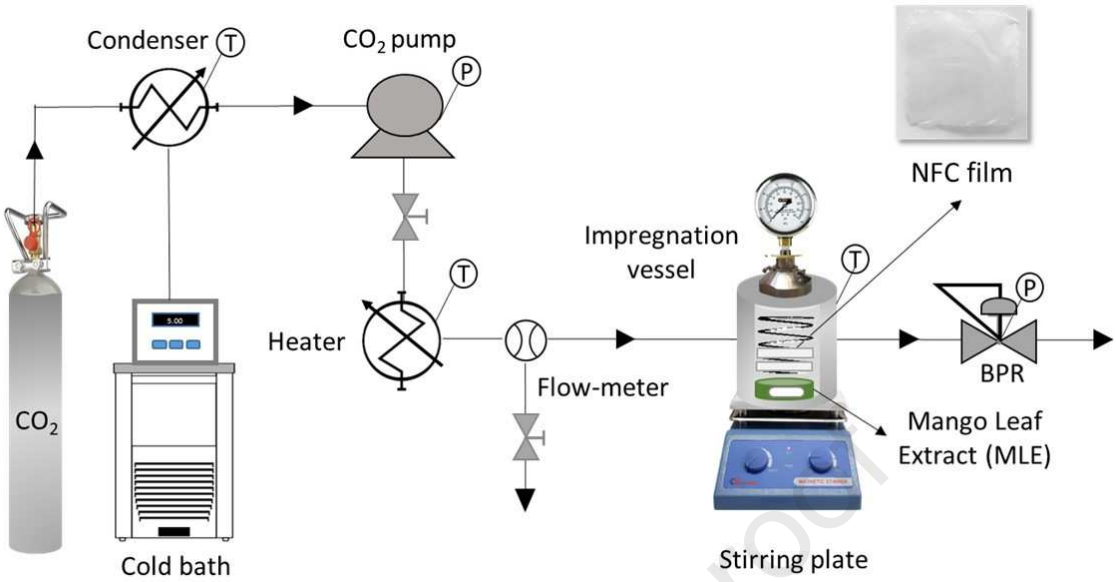

957 **Fig. 1**. Scheme of the supercritical solvent impregnation (SSI) set-up.

958

959

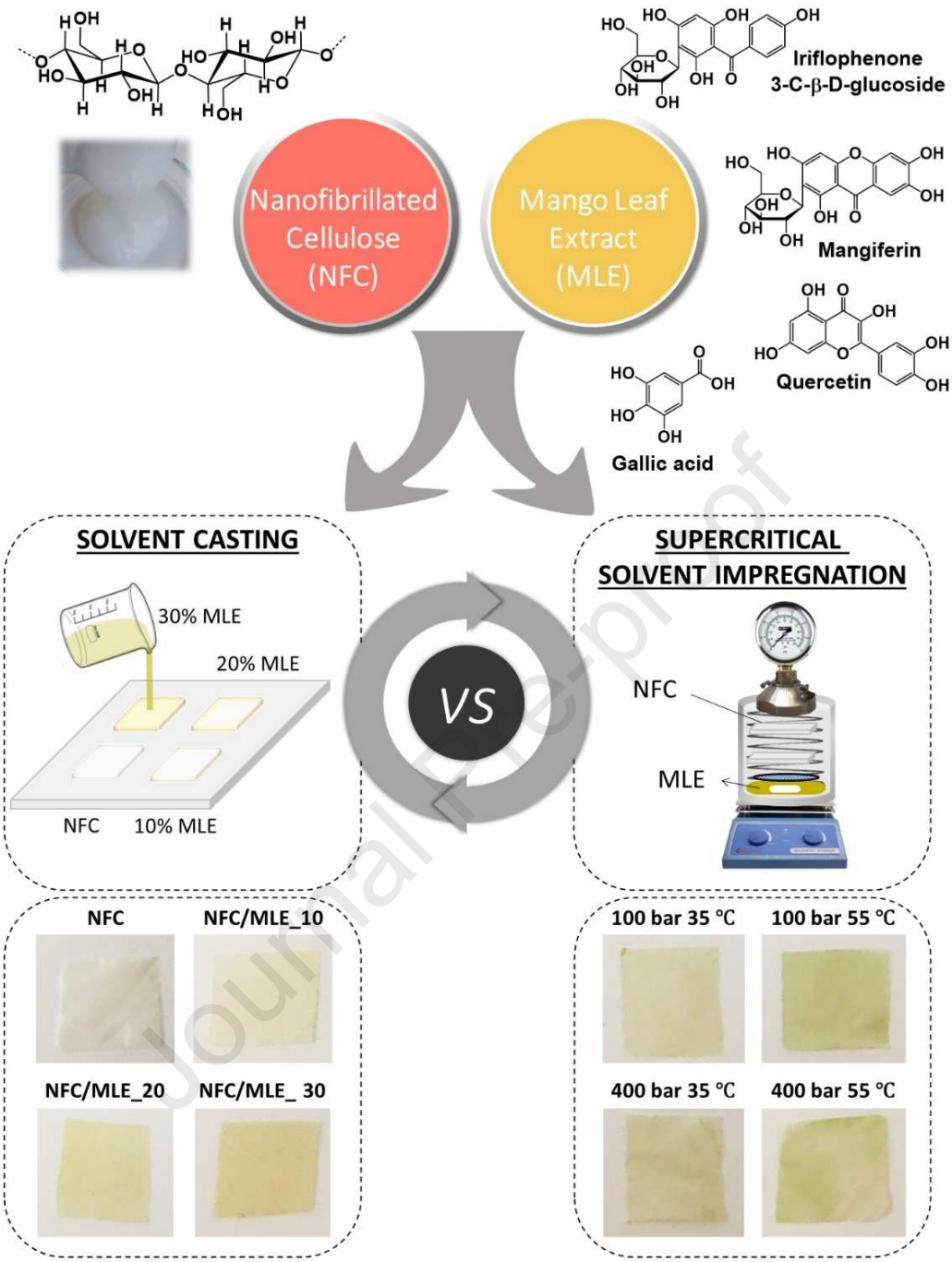

960 **Fig. 2**. Scheme illustrating the fabrication of the biobased NFC/MLE-based films (10
961 wt.% of glycerol) via solvent casting and SSI film-processing methodologies.

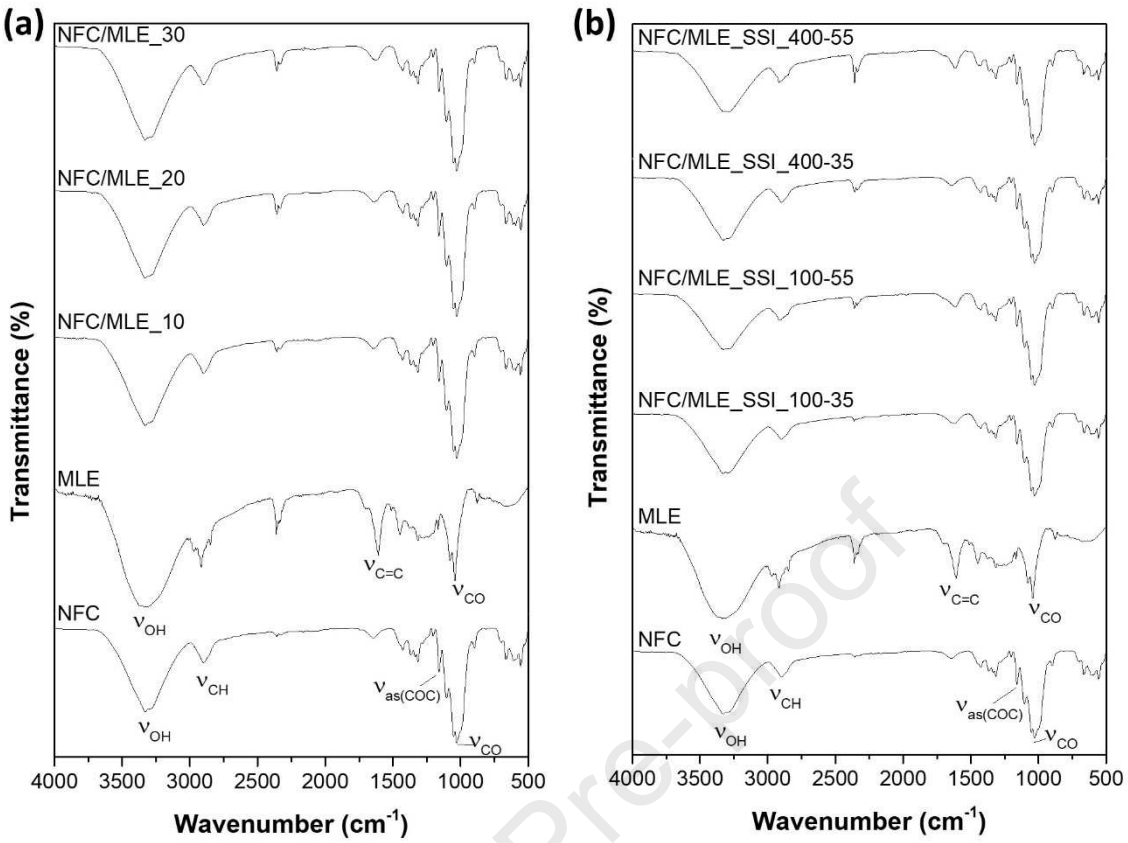

962 **Fig. 3**. FTIR-ATR spectra (vibrational mode: ν = stretching) of the pure NFC film, the
963 crude MLE, and the NFC/MLE-based films prepared via solvent casting (a) and SSI (b)
964 film-processing methodologies.

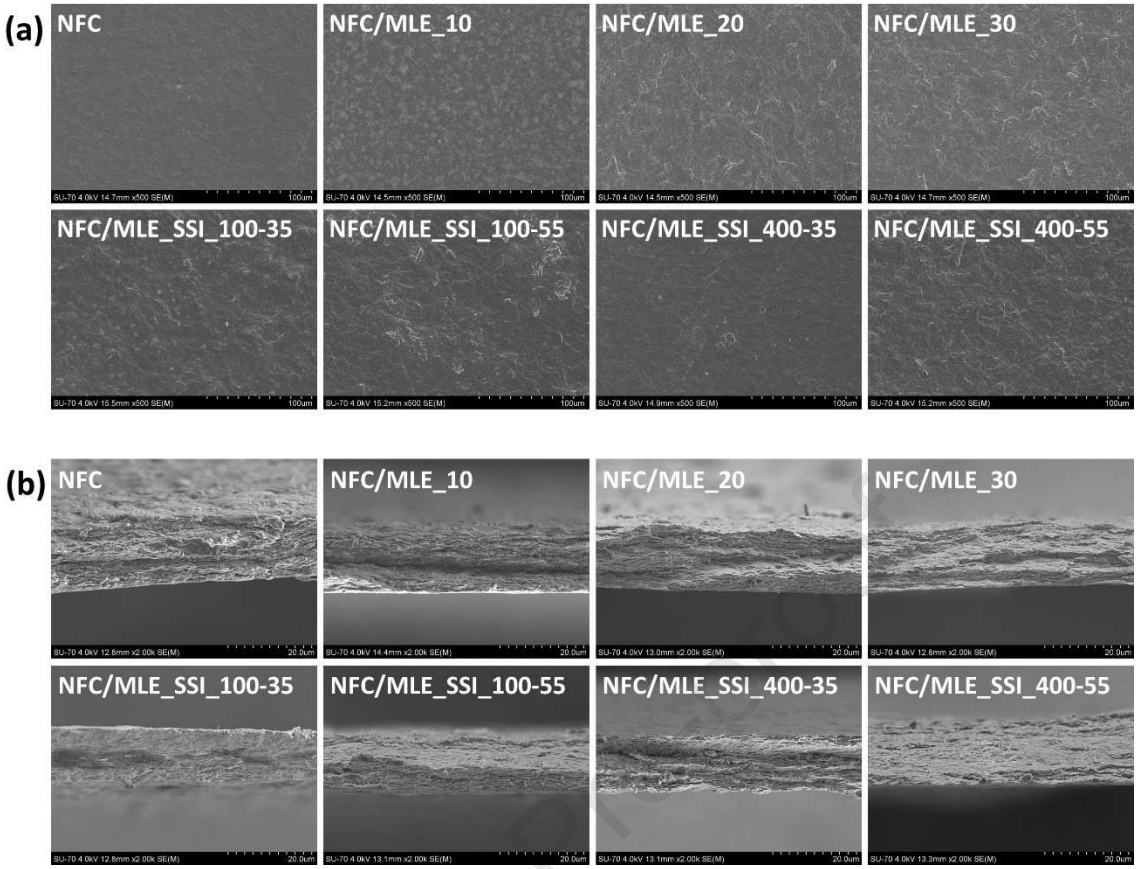

965 **Fig. 4**. SEM micrographs of the (a) surface and (b) cross-section of the NFC-based
966 films.

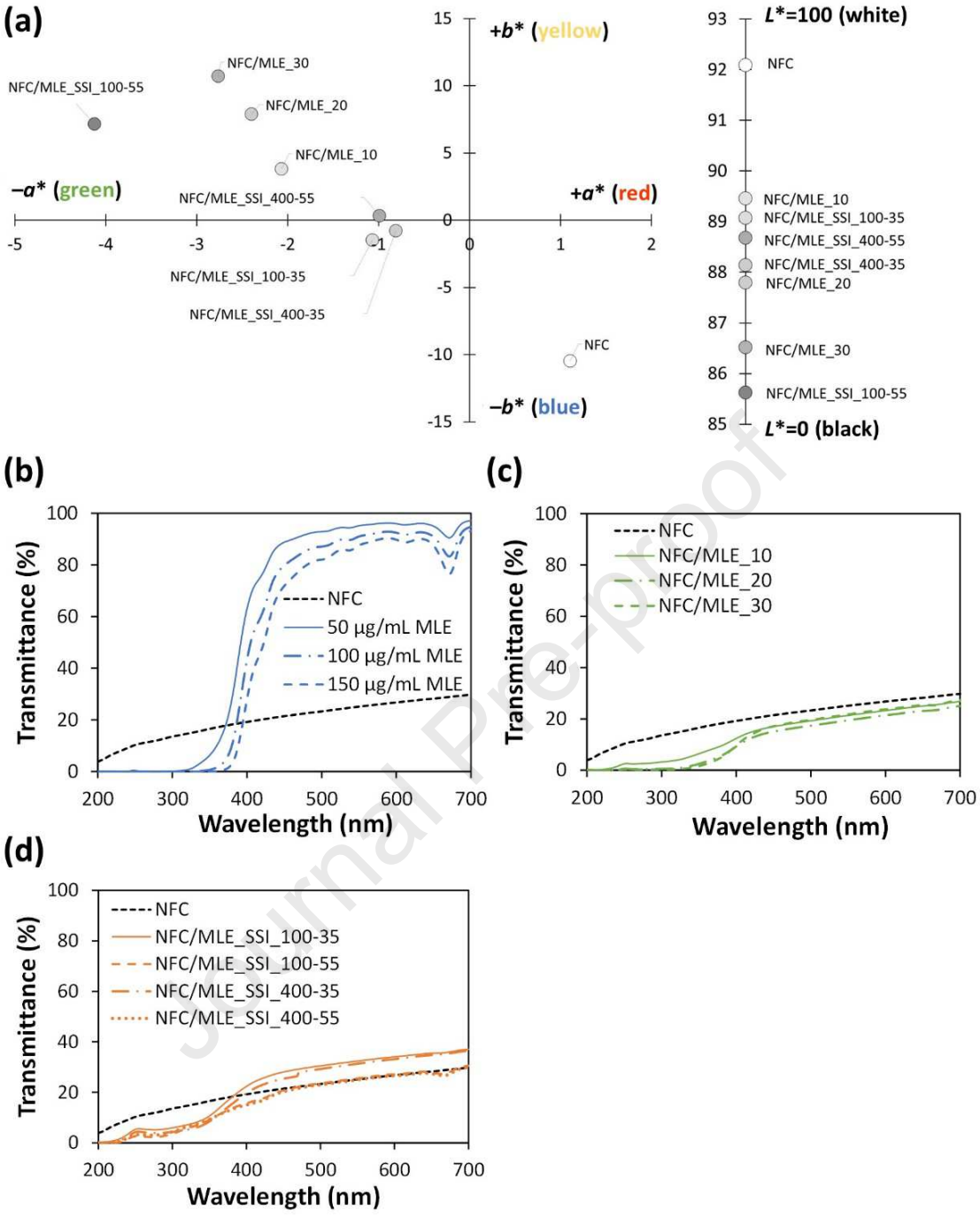

967 **Fig. 5**. (a) CIELab coordinates of the NFC-based films prepared by solvent casting and
968 SSI film-processing methodologies, (b-d) UV-Vis spectra of (b) NFC and MLE at
969 different concentrations, and NFC-based films prepared via (c) solvent casting and (d)
970 SSI film-processing methodologies.

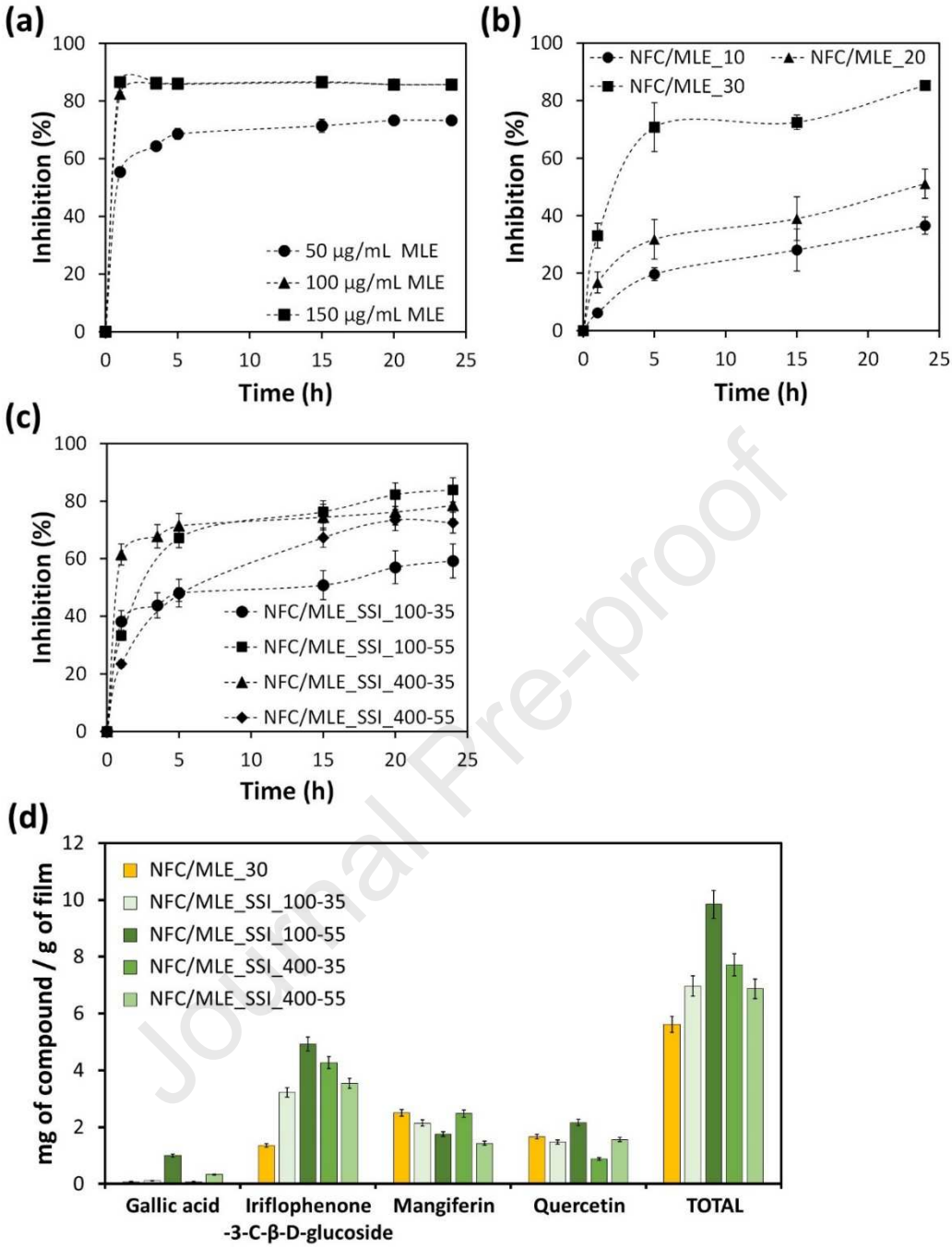

971 **Fig. 6**. Antioxidant capacity of the (a) pure extracts, and the NFC-based films prepared
972 via (b) solvent casting and (c) SSI film-processing methodologies, and (d) summary of
973 the phenolic composition, in terms of gallic acid, iriflophenone 3-C-β-D-glucoside,
974 quercetin, and mangiferin, of the NFC/MLE-based films obtained by solvent casting
975 and SSI film-processing methodologies (the standard deviation in the duplicates was
976 lower than 5%).

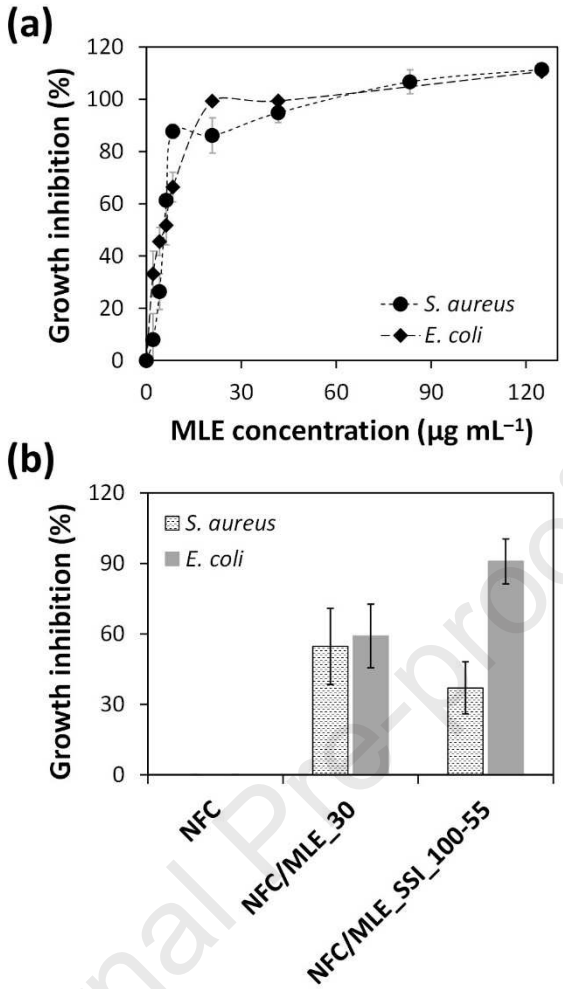

977 **Fig. 7**. Antimicrobial activity against gram-positive (*S. aureus*) and gram-negative (*E.*
978 *coli*) bacteria of the (a) pure MLE and (b) the NFC, NFC/MLE_30 and
979 NFC/MLE_SSI_100-55 films.

980

981 **Tables**

982

983 **Table 1**. List of the NFC-based films fabricated via solvent casting and SSI, with the
984 corresponding composition and thickness values.

	Films	Mass of NFC (mg)	Volume of MLE (mL)[1]	Mass of MLE (mg)	Thickness (μm)
CASTING	NFC	50	–	–	17±1
	NFC/MLE_10	50	0.090	4.95	18±1
	NFC/MLE_20	50	0.180	9.90	18±1
	NFC/MLE_30	50	0.270	14.85	18±1
SSI	NFC/MLE_SSI_100-35	50	5.0	275.0	19±1
	NFC/MLE_SSI_100-55	50	5.0	275.0	19±1
	NFC/MLE_SSI_400-35	50	5.0	275.0	19±1
	NFC/MLE_SSI_400-55	50	5.0	275.0	19±1

985 [1] the concentration of the MLE ethanolic solution is 55 g L^{-1}, and the 5.0 mL was used
986 for the impregnation of two NFC films (5×5 cm^2 each) films.

987 **Table 2**. TGA data of the NFC-based films prepared via (a) solvent casting and (b) SSI
988 film-processing methodologies.

	Films	T_{di} (°C)	T_{dmax} (°C)	Final residue (%)
CASTING	NFC	285	356	15.6
	NFC/MLE_10	273	350	12.9
	NFC/MLE_20	275	350	14.0
	NFC/MLE_30	272	351	15.4
SSI	NFC/MLE_SSI_100-35	259	343	19.6
	NFC/MLE_SSI_100-55	263	346	17.7
	NFC/MLE_SSI_400-35	265	346	16.3
	NFC/MLE_SSI_400-55	265	348	15.2

989 **Table 3**. Young's modulus, tensile strength, and elongation at break of the NFC-based
990 films prepared via solvent casting and SSI film-processing methodologies.*

	Films	Young's Modulus (GPa)	Tensile strength (MPa)	Elongation at break (%)
CASTING	NFC	4.71 ± 0.45 [a]	59.7 ± 3.9 [a]	3.48 ± 0.95 [a]
	NFC/MLE_10	4.98 ± 0.61 [a]	50.2 ± 4.5 [b]	2.82 ± 0.93 [b]
	NFC/MLE_20	5.46 ± 0.57 [c]	60.8 ± 8.4 [a]	2.51 ± 0.69 [b]
	NFC/MLE_30	5.64 ± 0.61 [d]	60.4 ± 7.4 [a]	2.28 ± 0.65 [c]
SSI	NFC/MLE_SSI_100-35	5.12 ± 0.22 [b]	52.1 ± 2.3 [b]	3.46 ± 0.65 [a]
	NFC/MLE_SSI_100-55	5.02 ± 0.52 [a]	57.2 ± 3.9 [a]	3.28 ± 0.94 [a]
	NFC/MLE_SSI_400-35	5.43 ± 0.12 [c]	58.3 ± 4.6 [a]	3.36 ± 0.73 [a]
	NFC/MLE_SSI_400-55	5.70 ± 0.21 [d]	59.4 ± 3.2 [a]	3.64 ± 0.91 [a]

991 * All values are expressed as means ± SD and the values in the same column followed
992 by distinct letters (a,b,c,d) are significantly different (p<0.05) as determined from the
993 statistical analysis.

Highlights

- Nanobrillated cellulose (NFC) films loaded with mango leaf extract (MLE) were prepared.
- Supercritical solvent impregnation and solvent casting film-processing were compared.
- Free-standing NFC/MLE films show UV-light protection and antioxidant properties.
- Films with antimicrobial activity against gram-positive and gram-negative bacteria.
- Active NFC/MLE sustainable films with potential for active food packaging.

Declaration of interests

☒ The authors declare that they have no known competing financial interests or personal relationships that could have appeared to influence the work reported in this paper.

☐The authors declare the following financial interests/personal relationships which may be considered as potential competing interests: